The International Archives of the Photogrammetry, Remote Sensing and Spatial Information Sciences, Volume XLVIII-G-2025
ISPRS Geospatial Week 2025 “Photogrammetry & Remote Sensing for a Better Tomorrow…”, 6–11 April 2025, Dubai, UAE

Comparison of TLS and photogrammetric workflows for tracking Alpine rock slope failures

Lukas Raffl[1], Lukas Lucks[1], Christoph Holst[1]

[1] Chair of Engineering Geodesy, TUM School of Engineering and Design, Technical University of Munich (TUM)
80333 Munich, Germany
(lukas.raffl, lukas.lucks, christoph.holst)@tum.de

Keywords: Geo-monitoring, laser scanning, feature tracking, point clouds, mass movements, deformation analysis

Abstract

This paper presents a comparative analysis of photogrammetric and Terrestrial Laser Scanning (TLS) workflows for geo-monitoring alpine rock slope failures, focusing on the quality of the resulting point clouds and 3D displacement vectors. We compare two tracking workflows, a patch-based approach for TLS point clouds and a 2D feature-based method for photogrammetry. We evaluate both methods using data from the Hochvogel Mountain test site, collected across two measurement epochs. The results demonstrate that both TLS and photogrammetry effectively detect ongoing movement patterns down to a few millimeters, with similar accuracy despite slight differences in noise levels. Both methods offer high spatial resolution and sensitivity to small-scale displacements, showing strong agreement with reference measurements from tachymetry. Differences mainly arise in the spatial distribution: the TLS method is sparse in planar areas but very regular, while the photogrammetric method yields a significantly higher number of vectors, concentrated in regions with strong texture variation, but also includes more outliers.

1. Introduction

The monitoring of alpine rock slope failures presents significant challenges due to the complex and irregular structure of rock surfaces, combined with often limited accessibility to these regions. Accurate tracking is further complicated by the slow movement rates typically observed, which are often on the scale of millimeters per month. To comprehensively capture such movements, a dense spatial coverage is essential. Terrestrial Laser Scanning (TLS) and image-based photogrammetry are both well-suited for this task, as they allow the creation of high-resolution 3D reconstructions in the form of point clouds (Lucks et al., 2024; Raffl and Holst, 2024). However, they differ in some practical aspects like costs, transportability, acquisition time and lighting conditions.

A significant challenge in both measurement techniques is the need for point correspondences between point clouds from different epochs. This is essential for the tracking of ongoing movements. Common strategies to identify correspondences include distance-based approaches or estimating small local models (Lague et al., 2013; Zahs et al., 2022; Yang and Schwieger, 2023). However, these methods often fail to fully capture the ongoing movement or provide results with limitations. An alternative approach involves feature-based tracking, which can be applied in both 2D (Ioli et al., 2023) and 3D domains (Gojcic et al., 2021). For photogrammetry, dense matching algorithms can generate dense 3D point clouds, while for TLS, reprojecting data into 2D rasters or images allows for similar feature detection and matching (Hosseini et al., 2024).

In this paper, a comparison between the measurement techniques TLS and photogrammetry is presented using data from Hochvogel Mountain. In order to monitor the summit of Hochvogel, we employed TLS and terrestrial cameras to generate point clouds from different epochs. This test site has already been the subject of past research. Several results from geodetic network measurements and photogrammetry have been published already (Raffl and Holst, 2024; Barbosa et al., 2024; Lucks et al., 2024; Raffl and Holst, 2022; Lucks et al., 2022; Raffl and Wunderlich, 2020; Leinauer et al., 2020). Also, comparisons between point clouds from laser scanning and photogrammetry already exist (Dinkel et al., 2020). However, in this paper, we now introduce the results of using a common terrestrial laser scanner for scanning dense point clouds. In contrast, previous studies were restricted to a scanning total station, which could only acquire point clouds with lower spatial density. This also allows the introduction of a new measurement epoch and an advanced processing pipeline. Comparisons will be more detailed and comprehensive to even better understand the differences in outcome between the two measurement techniques.

For the calculation of displacement vectors, we introduce and use two workflows that have been specifically developed for tracking alpine rock slope failures. Both workflows aim at a higher spatial resolution compared to signaled target points, derived from a fully automatic workflow, sensitive for the detection of movements in the range of millimetres to centimetres, and statistically tested for significance in terms of rigorous deformation analysis. The first is a 3D patch-based method (Raffl and Holst, 2024) for TLS point clouds. Distinct point cloud patches are identified within each epoch, which serve as proxies for the missing point correspondences. The second approach leverages a photogrammetric workflow, where 2D image features are identified and matched across images within and between epochs. Matched feature points are projected onto reconstructed point clouds to calculate 3D deformation vectors (Lucks et al., 2024). Both workflows address the limitations of traditional methods, such as the M3C2 (Lague et al., 2013) algorithm, by providing a 3D displacement vector field of the study area. An overview of both methods and their respective results is provided in figure 1.

After introducing the two workflows in more detail in section 2, we briefly describe the test site and the measurement setup we used in the two measurement epochs (section 3). In section 4, we first conduct a comparative analysis of the resulting

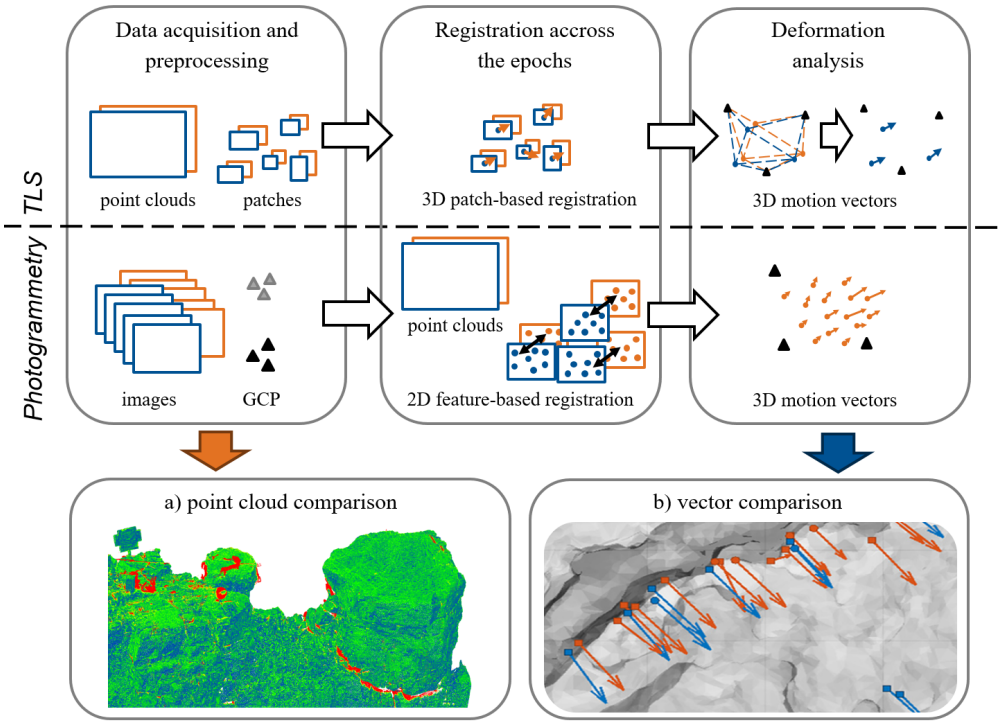

Figure 1. Main steps of the workflow for tracking Alpine rock slope failures, with TLS illustrated in the upper row and photogrammetry in the lower row. The results are shown as a point cloud-based comparison (a) and a comparison of 3D displacement vectors derived from the two workflows (b).

point clouds to evaluate resolution, coverage, noise levels, and the geometric deviations between the point clouds. These metrics are assessed by analyzing specific parts of the point clouds. Geometric deviations are quantified using the M3C2 algorithm, which identifies differences between the two datasets, providing insights into their compatibility and reliability. Afterwards we compare the results of the two tracking workflows. Displacement vectors from both methods are compared to each other and to reference vectors derived from network-based monitoring (total station and GNSS). Finally, we conclude our paper in section 5 and give an outlook on further research.

2. Tracking of Alpine rock slope failures

In this study, two tracking methods for 3D motion estimation are presented: Patch-based tracking and 2D feature-based tracking. Both approaches aim to improve point correspondences across epochs, resulting in a vector field representing the ongoing 3D displacement. The following sections provide a detailed description of the two methods.

2.1 Patch-based tracking

The workflow presented in Raffl and Holst (2024) has been extended to enable fully automated patch selection and processing for TLS. A key advancement is the use of the Extended Gaussian Image (EGI) for automatic identification of suitable patches, eliminating the need for manual preselection. The main steps of the used workflow for patch-based tracking are:

1. **Preprocessing of point clouds:** All the scans of each epoch are georeferenced using targets. Instead of merging all scans of an epoch into a single point cloud, each scan remains separate. A regular grid is then used to define random candidates for patches in each scan.
2. **Patch selection using the Extended Gaussian Image (EGI):** The EGI is created for each patch candidate to automatically select only those patches suitable for Iterative Closest Point (ICP) matching. Within this process the surface normal distributions are analyzed to assess geometric variation, ensuring that only patches with sufficient structure for stable matching are used (Raffl et al., in preparation).
3. **ICP matching and Monte-Carlo Simulation:** Following the supervised approach introduced in Raffl and Holst (2024), ICP matching is now applied systematically to all corresponding patch pairs. This includes both patch pairs from different epochs as well as patches scanned from different stations within the same epoch. Since scans are not merged, each station’s perspective remains distinct, allowing ICP to provide multiple independent observations of the same patch. This redundancy is a key advantage over conventional point-cloud-based monitoring methods, where scans are typically combined into a single point cloud per epoch (Lague et al., 2013; Holst et al., 2021; Winiwarter et al., 2021; Yang and Schwieger, 2023).
   To ensure reliability, each patch pair undergoes an individual Monte Carlo simulation. Small random displacements are introduced, and the ICP algorithm is repeatedly applied. The resulting transformation stability is analyzed to identify unreliable patch pairs, which are then discarded.
4. **Redundancy filtering and network integration:** A major advantage of the proposed approach is that redundant observations of the same patches from different stations are available. This is only possible because individual scans are preserved instead of being merged. Our approach enables a redundancy-based filtering step: only patches that were successfully matched between a minimum number of stations within each epoch are used. This ensures

higher reliability in the final network adjustment.

5. **Network adjustment and deformation analysis:** The final set of virtual points is integrated into a geodetic network adjustment (Raffl and Holst, 2024). The increased redundancy improves both the precision and statistical significance of the derived deformation vectors, providing a robust framework for geodetic deformation analysis.

This extension significantly enhances the automation and reliability of the original method. A full description of the initial workflow can be found in Raffl and Holst (2024), while a complete description of this extended approach will be provided in Raffl et al. (in preparation).

2.2 2D feature-based tracking

For image-based geo-monitoring, collections of overlapping images are captured for each epoch. For an accurate registration, a set of Ground Control Points (GCPs) is required. Following the steps of the Structure-from-Motion (SfM) workflow, we compute a dense point cloud while simultaneously estimating the camera positions, their accuracies, and a set of 2D feature points with corresponding descriptors. To achieve efficient and accurate matching, we utilize the known camera geometries.

Starting from the feature points in the reference epoch, we project these points into the images of the next epoch. This approach constrains the search radius for feature matching by defining a limit around the projected points that correspond to the maximum expected displacement. For feature extraction, we employ the classical SIFT algorithm Lowe (2004). While deep-learning-based approaches generally provide more robust matching, SIFT offers higher accuracy in feature localization within images Morelli et al. (2024), eliminating the need for additional subpixel refinement. Note that the set of features used for registration within an epoch and across epochs does not necessarily have to be the same.

Significant changes between epochs, such as snowfall or erosion, can create large areas where feature tracking is not possible. However, features in these regions remain crucial for the registration of individual epochs. For each successfully matched feature point, the 3D coordinates are calculated using triangulation. Based on these coordinates, the matching correspondences, and the 3D points from the reference epoch, the displacement vectors can be determined. For more information about the workflow, we refer to Lucks et al. (2024).

3. Experiments and test site

Mt. Hochvogel, located on the German-Austrian border in the Allgäuer Alps, is a geologically active site known for its susceptibility to a huge rockfall event. Characterized by brittle, tectonically stressed dolomite, the mountain has been experiencing significant erosion, with an enormous cleft forming at its summit over recent decades. This cleft, which splits the mountain into two parts, is a source of considerable concern, as the southern section is at risk of breaking off (figure 2). Previous research on the site has already included geodetic network measurements and photogrammetric analyses, along with comparisons of point clouds obtained from scanning total stations and photogrammetry. In this study, we introduce two measurement epochs from 2021 and 2023, focusing on the unstable sidewall of the cleft (figure 2, yellow box).

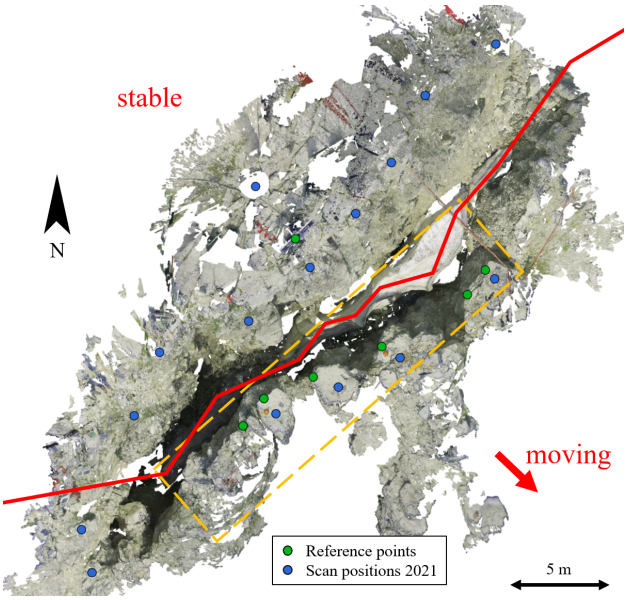

Figure 2. An overview of the test site at Mt. Hochvogel, highlighting both stable and moving areas and showing the locations of reference points and the scan positions from 2021. The yellow box indicates the region of interest for this study.

For TLS, a Leica RTC360 laser scanner was used in both measurement campaigns. Scans were taken from 15 and 13 positions, respectively, to ensure sufficient coverage of the area. The scans were captured with the highest possible resolution of 3 mm at 10 meters (table 1). For registration, the scans were aligned using the ICP algorithm and georeferenced with 5 or 6 targets. These targets were measured with a total station and GNSS within the existing geodetic network to ensure accurate positioning.

In the patch-based analysis, overlapping patches with a diameter of 400 mm were initially created on the basis of a 200 mm grid. This patch size was chosen to match the rock structure of Hochvogel. For optimizing processing, the point clouds were downsampled to a point spacing of 10 mm, as sufficient details were still maintained for ICP matching. After Monte Carlo simulation and ICP matching, only the patches that were visible from at least two scan positions in each epoch were selected. This filtering step ensured reliable correspondences for further analysis.

	TLS	**Photogrammetry**
Sensor	Leica RTC360	Sony Alpha 7R II
Resolution	3 mm @ 10 m	7952x5304 px
# 2021/2023	15/13 scans	295/140 images

Table 1. Technical data of the used sensors.

For photogrammetric monitoring in both epochs, high-resolution images were captured (table 1) following the same strategy as in previous studies (Lucks et al., 2024). However, in 2023, fewer images were recorded since the lower part of the cleft was covered with snow. The campaign took place a few weeks earlier than the TLS observation. For registration, ten GCPs were used, assuming an absolute positioning accuracy of 4 mm. To implement the Structure-from-Motion workflow, we used the software Pix4D©, utilizing the resulting accuracies for variance propagation to estimate the displacement uncertainty (Strecha, 2014), while the computation of SIFT feature vec-

tors was performed using the OpenCV Python library (Bradski, 2000).

For the comparison of both tracking methods, we only consider key points that are visible in at least three images. Additionally, all points with a reprojection error greater than one pixel are eliminated. Since the recorded data covers the entire cleft, we focus on a subset of images that provide good coverage of the region of interest (figure 2) for the calculation of feature tracking.

4. Results and discussion

In the following sections, the differences between the point clouds of the two measurement techniques will first be analyzed. Then, the results of the two tracking methods will be examined and compared with reference measurements.

4.1 Comparison of resulting point clouds

Both measurement techniques provided a valuable point cloud of the test site. All four point clouds cover the region of interest very well and represent a high amount of detail. The completeness strongly depends on the number of scans, respectively, images, and sensor positions. Since the camera is more mobile than the laser scanner, it generally allows for better coverage of all areas. However, it is more susceptible to shadows and changing lighting conditions. As a result, in our case, the photogrammetric point clouds have slightly more omissions compared to the TLS point clouds.

To assess differences in quality, we calculate M3C2 distances within each epoch between the TLS and photogrammetric point clouds. The M3C2 distances reveal a high correspondence between the two point clouds in both epochs. The median distances are 2.0 mm and -1.3 mm with a standard deviation of 3 mm and 4 mm (epoch 2021 and 2023) (see figure 3 blue histograms). However, the comparison reveals minor discrepancies in registration. This can be explained by the limited accuracy of the used targets and GCPs of 4 mm. Considering this, the misalignment is not significant within these limits.

For further comparison, however, we improve the alignment using the Iterative Closest Point (ICP) algorithm and recalculating the M3C2 distances. Figure 3 also depicts the deviations between the point clouds after the refined alignment (orange histogram) and shows that the consistency between the point clouds improves after alignment as the distances generally got smaller to a median distance of 1.0 mm and 0.6 mm with a standard deviation of 3 mm for both epochs (2021 and 2023).

The remaining differences are visualized in figure 4. The distribution reveals a clear depth-dependent gradient, with significantly lower deviations in the upper part of the column. Several factors may contribute to these residual differences: Increasing distance from the sensor, varying lighting conditions, and the lack of ground control points (GCPs) in the lower region during photogrammetric reconstruction may all play a role. Additionally, the lower part of the area is observed less frequently, and TLS accuracy is inherently angle-dependent (Wujanz et al., 2017). Apart from these systematic errors, bigger differences are observed at edges and cracks. Larger discrepancies appear at sharp edges, where mismatches against the sky lead to artefacts in the photogrammetric point cloud.

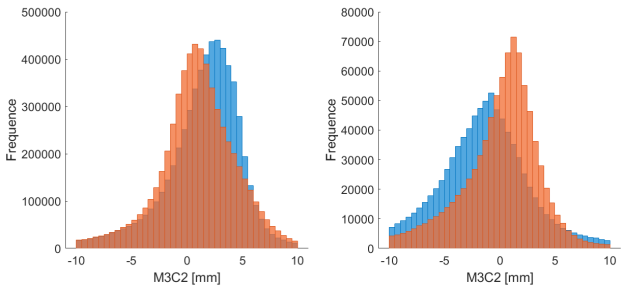

Figure 3. M3C2 distances between TLS and photogrammetric point clouds within the same epoch 2021 (left) and 2023 (right) for the origin points (blue) and aligned using ICP (orange).

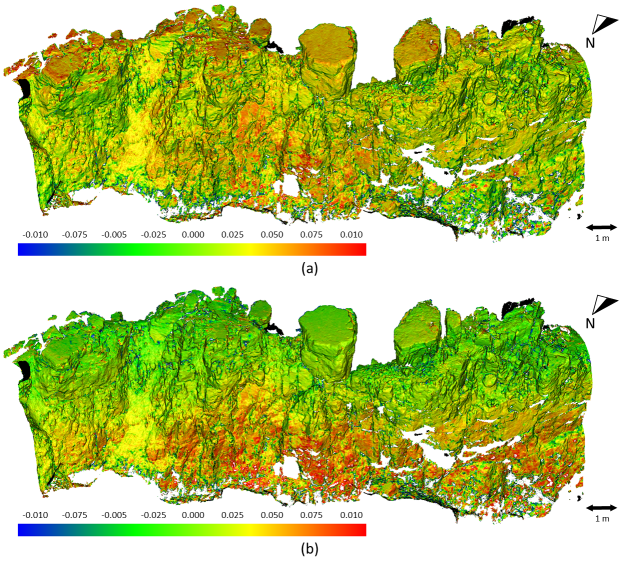

Figure 4. M3C2 distances between TLS and photogrammetric point clouds for the epoch 2021 before (a) and after the alignment (b) with ICP.

To gain further insights into the general noise level of the point clouds, we again use the results of the M3C2 algorithm. For epoch-wise point cloud comparisons, the M3C2 algorithm not only calculates distances as an indicator of ongoing deformation, but also provides an uncertainty value based on the local plane estimation for each core point. We use this value as a metric for the noise level.

	TLS	Photogrammetry
Completeness	very high	high
Noise (2021/2023)	6 mm / 7 mm	6 mm / 8 mm
Resolution	< 3 mm	< 3 mm

Table 2. Qualitative and quantitative comparison of the point clouds.

The mean scatter of all core points for each point cloud is listed in table 2. It can be observed that the point clouds from 2023 exhibit slightly higher noise levels than the point clouds from 2021. In general, both measurement techniques demonstrate a very similar noise level. It is important to note that the range of 6–8 mm does not exclusively represent noise but also indicates how well surfaces can be locally approximated by planes. Therefore, these values should be used primarily for comparing sensors rather than as an absolute noise meas-

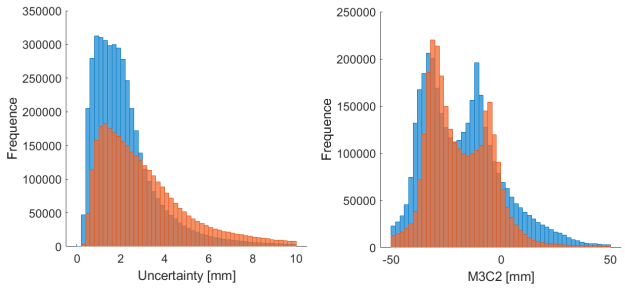

Figure 5. Comparison of TLS (blue) and Photogrammetry (orange): M3C2 uncertainties (left) and M3C2 distances (right) between 2021-2023.

urement. A similar trend is evident when analyzing the uncertainties of the M3C2 distances (figure 5, left), where the photogrammetric point clouds show slightly greater uncertainties.

Overall, the analysis shows that the primary source of deviations is registration error; however, the point clouds generally align well, mostly in the range of a few millimeters with only small differences in the noise level.

The results of the point cloud comparison between the 2021 and 2023 epochs are shown in figure 5 (right). Both methods reveal the same movement pattern, characterized by two distinct peaks corresponding to horizontal and vertical displacement of approx. 30 mm and 8 mm. These findings align with previous studies (Lucks et al., 2022), confirming that the movement is continuously ongoing. While both approaches successfully capture the displacement, small differences in the peak values of 2 mm (larger peak) and 6 mm (smaller peak) are observed, which are likely explained by slight deviations in the registration.

4.2 Comparison between the tracking methods

The deformation results from both methods are compared with each other and with reference data from a total station and GNSS network. The network-based monitoring approach is well-established and is assumed to provide high-quality results (Ogundare, 2016, p. 267ff.). Within the monitoring network at Hochvogel, there are several marked points located in the defined region of interest. However, it is important to note that these results also have limited accuracy, which must be considered when interpreting the comparison.

To compare the vectors from our approaches with the reference vectors, we search for the nearest vector to each marked point and compare both magnitude and direction. A visual comparison is shown in figure 6 and the resulting magnitudes, including their standard deviations, are listed in table 3. The comparison reveals strong correspondences across our approaches and with the reference vectors. However, as expected, the M3C2 vectors display a distinct pattern, as the actual movement does not occur in the normal direction of the surface.

A major advantage of both methods is the inclusion of error propagation, which provides information about the accuracies and enables statistical significance tests of the result. In the present case, all vectors within the region of interest are significant. Table 3 reveals that the vectors from patch-based tracking

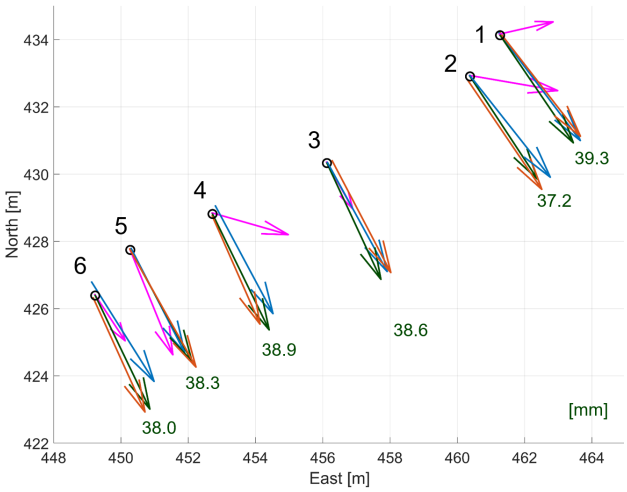

Figure 6. Comparison of displacements calculated with M3C2 (magenta), patch-based method (blue) and feature-based method (orange) to reference from marked points (green). Green values quantify the length of the reference vectors in [mm].

have a nominal higher accuracy than the total station measurements on the reflective tapes (marked reference points). The standard deviation of the feature-based vectors, however, is higher. This is partly due to the fact that the evaluation strategies and the associated error calculations follow different approaches.

ID	$d_{\text{reference}}$	d_{patch}	d_{feature}	d_{M3C2}
1	39.3 ± 3.3	40.7 ± 2.1	39.7 ± 7.3	16.8
2	37.2 ± 3.3	38.9 ± 2.1	39.3 ± 6.2	27.1
3	38.6 ± 3.3	37.7 ± 2.6	38.0 ± 5.2	25.3
4	38.9 ± 3.3	37.0 ± 2.4	35.4 ± 4.1	26.7
5	38.3 ± 3.3	35.5 ± 2.1	40.6 ± 4.1	36.9
6	38.0 ± 3.3	35.5 ± 3.5	37.6 ± 4.4	21.8

Table 3. Motion of the reference points, patch-based, feature-based, and M3C2-based measurements between 2021 and 2023 in millimeters.

In the TLS workflow, the virtual target points are converted into polar observations at the end and analysed in a strict deformation analysis according to Pelzer (1971). Here, all observations from both epochs are combined into a common network and a free network equalisation with identical dates takes place. As a result, the relative covariance matrices of the coordinate differences are obtained directly.

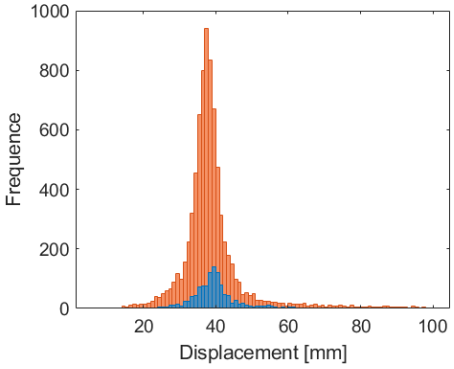

Figure 7. Length of the calculated displacement vectors using patch-based (blue) and feature-based approach (orange)

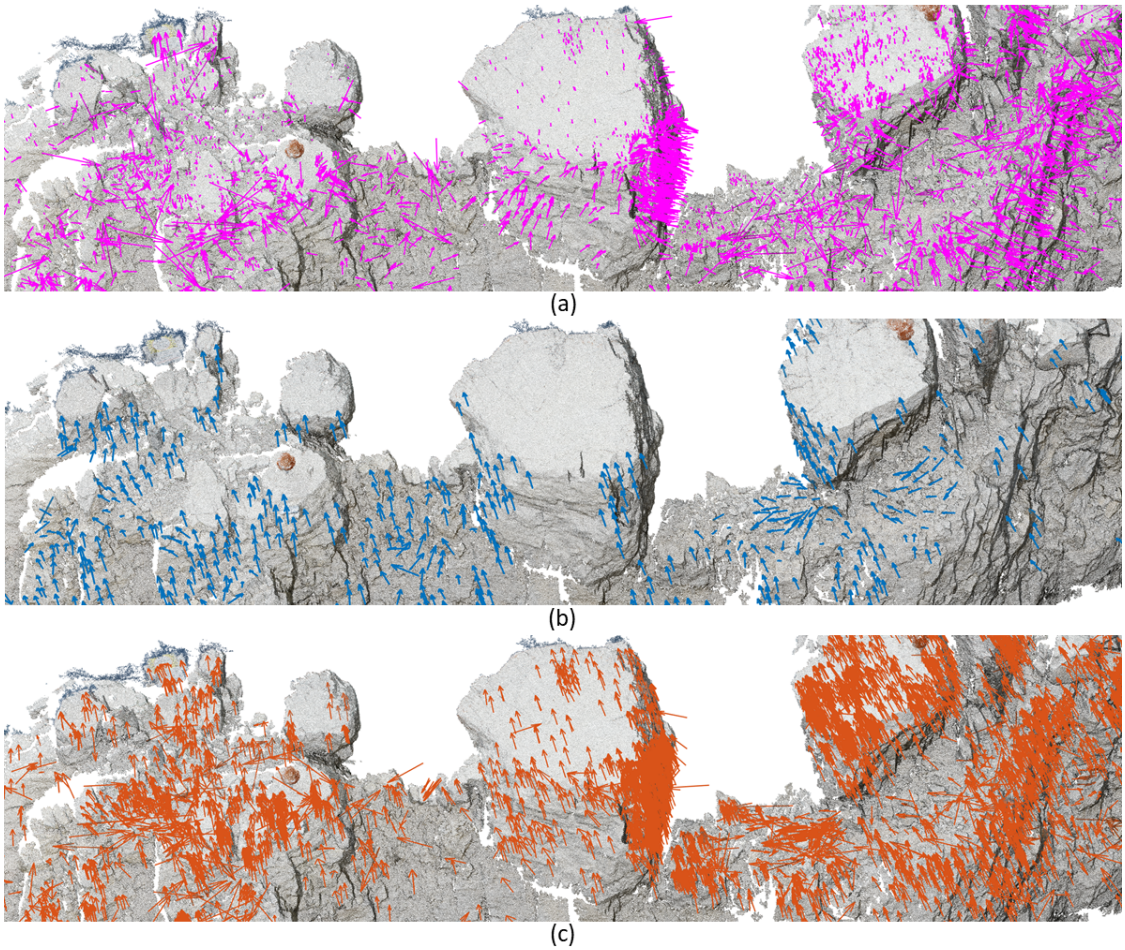

Figure 8. Calculated displacement vectors with M3C2 (purple), patch-based (blue) and feature-based approach (orange), visualized on a subset of the 2023 point cloud. Vectors are scaled by a factor of six.

With the photogrammetric approach, on the other hand, a bundle-block adjustment is first carried out separately for both epochs. An accuracy specification must already be made for the GCPs, which is then propagated to the estimated points. The coordinate differences are then formed and the single point accuracy is propagated once again. As the accuracy of the GCPs, in this case, was assumed to be very pessimistic at 4 mm, this has a corresponding effect on the result of the vectors. The assumed point accuracy corresponds to the absolute accuracy of the points in the superordinate coordinate system. The relative accuracy of the points between the epochs can be assumed to be much more optimistic, so the actual accuracy of the vectors can also be assumed to be many times better. This is further confirmed by the resulting vectors, which match the reference vectors very well.

When comparing all vectors from the TLS and photogrammetric methods, a clear difference in vector quantity becomes evident. Within the defined region of interest, the patch-based approach yields 1,159 vectors, while the feature-based method produces 7,966. This discrepancy arises because the vector density in the patch-based approach is constrained by the patch size, whereas photogrammetry establishes correspondences at the pixel level. The histogram of vector lengths in figure 7 shows that all vectors follow the magnitude indicated by the reference vectors.

However, figure 8 clearly illustrates the different spatial distributions of vectors within the area. The patch-based ICP matching of the scan data does not generate vectors on flat surfaces, such as the tops of the large boulders. In contrast, the photogrammetric approach performs well in these areas as long as sufficient texture is present. On the left side of the scan area, however, the feature-based method appears to produce a noisier result with a high number of outliers. Due to the raster-based structure of the patch-based method, its vectors create a smoother representation of the movement pattern in this area. Overall, the vectors from the M3C2 algorithm provide the least insight into the ongoing movement patterns. In this study, both the patch-based and feature-based approaches helped uncover a new movement pattern on the right side of the region of interest, where no marked points are available and M3C2 does not provide precise information.

The number, density, and distribution of vectors in both approaches depend strongly on the chosen parameters and input data. For the TLS approach, for example, the patch size could be further reduced in combination with a lower downsampling rate of the point clouds. This would increase the number of patch candidates while also enhancing sensitivity to smaller structures. In other words, a smaller patch size makes ICP more responsive to finer geometric features. As a result, more patches pass the Monte-Carlo Simulation, even in flatter areas.

However, despite the significantly lower number of vectors in the TLS-based monitoring, the coverage of the moving area re-

mains sufficient. We divided the region of interest into 200-mm-patches, corresponding to the minimum patch spacing, and analyzed for both of the methods whether each patch contained a displacement vector. The results show that the patch-based approach covers 47% of the area, while the feature-based approach covers 44%. This indicates that, at a spatial resolution of 200 mm — which is entirely sufficient for the present use case — both methods provide similar coverage.

5. Conclusion and outlook

In this study, we compare photogrammetric and TLS workflows for geo-monitoring, focusing on the evaluation of the quality of the resulting point clouds and primarily analyzing the results of a 3D and a 2D tracking approach to estimate 3D displacement vectors. It can be concluded that both photogrammetric and TLS point clouds effectively detect ongoing movement patterns down to a few millimeters and yield comparable results.

Both approaches provide sufficient accuracy for this purpose. Photogrammetric point clouds exhibit slightly higher noise levels, but beyond the internal accuracy of the point clouds, alignment and georeferencing play a crucial role in the final results. Similar results occur for the 3D tracking of points. The absolute values of the 3D displacement vectors are highly consistent across both methods.

Differences primarily arise from the spatial distribution of the vectors. Patch-based approaches face challenges in flat areas, while feature-based methods rely on sufficient texture information. Although the number of vectors in TLS depends on resolution, feature-based approaches generally yield more vectors. However, these results tend to include more outliers and may require additional filtering, such as histogram filtering Hosseini et al. (2024).

Since the quality of the results is difficult to assess, the choice of method can be more oriented towards external factors during the measurement campaigns. Practical constraints, such as transport logistics, cost, and visibility/targeting limitations (e.g., pole-mounted versus fixed-position setups), should guide the selection of the most suitable method.

In the case of Mt. Hochvogel, the results demonstrate that both photogrammetric and TLS methods provide sufficient resolution to capture the ongoing displacement processes. The movement pattern is relatively uniform across the study area, which extends approx. 20 m. This indicates that a lower resolution would also be sufficient to detect the movement. At the same time, the high spatial coverage ensures that potential new movement patterns can be detected at an early stage in the coming years, providing valuable insights into the progression of the rock slope failure.

For future studies, increasing the resolution of displacement vectors would be of secondary importance compared to improving spatial coverage. Joint evaluation of both methods could enhance overall coverage and compensate for the limitations of individual techniques, leading to more robust results and reducing gaps in the data.

Funding

This research was partly funded by German Research Foundation (DFG) under grant number 490989047, DFG FOR 5455 ”TLS-Defo”.

References

Barbosa, N., Leinauer, J., Jubanski, J., Dietze, M., Münzer, U., Siegert, F., Krautblatter, M., 2024. Massive sediment pulses triggered by a multi-stage 130 000 m^3 alpine cliff fall (Hochvogel, DE–AT). *Earth Surface Dynamics*, 12(1), 249–269. https://esurf.copernicus.org/articles/12/249/2024/.

Bradski, G., 2000. The OpenCV Library. *Dr. Dobb’s Journal of Software Tools*.

Dinkel, A., Hoegner, L., Emmert, A., Raffl, L., Stilla, U., 2020. Change detection in photogrammetric point clouds for monitoring of alpine, gravitational mass movement. *ISPRS Annals of Photogrammetry, Remote Sensing and Spatial Information Sciences*, V-2-2020, 687-693.

Gojcic, Z., Schmid, L., Wieser, A., 2021. Dense 3D displacement vector fields for point cloud-based landslide monitoring. *Landslides*, 18.

Holst, C., Janßen, J., Schmitz, B., Blome, M., Dercks, M., Schoch-Baumann, A., Blöthe, J., Schrott, L., Kuhlmann, H., Medic, T., 2021. Increasing spatio-temporal resolution for monitoring alpine solifluction using terrestrial laser scanners and 3d vector fields. *Remote Sensing*, 13(6), 1192.

Hosseini, K., Reindl, L., Raffl, L., Wiedemann, W., Holst, C., 2024. 3D Landslide monitoring in high spatial resolution by feature tracking and histogram analyses using laser scanners. *Remote Sensing*, 16(1).

Ioli, F., Bruno, E., Calzolari, D., Galbiati, M., Mannocchi, A., Manzoni, P., Martini, M., Bianchi, A., Cina, A., de michele, C., Pinto, L., 2023. A replicable open-source multi-camera system for low-cost 4D glacier monitoring. *The International Archives of the Photogrammetry, Remote Sensing and Spatial Information Sciences*, XLVIII-M-1-2023, 137-144.

Lague, D., Brodu, N., Leroux, J., 2013. Accurate 3D comparison of complex topography with terrestrial laser scanner: Application to the Rangitikei canyon (N-Z). *ISPRS Journal of Photogrammetry and Remote Sensing*, 82, 10-26.

Leinauer, J., Jacobs, B., Krautblatter, M., 2020. Anticipating an imminent large rock slope failure at the Hochvogel (Allgäu Alps). *Geomechanics and Tunnelling*, 13(6), 597-603. https://onlinelibrary.wiley.com/doi/abs/10.1002/geot.202000027.

Lowe, D. G., 2004. Distinctive image features from scale-invariant keypoints. *International Journal of Computer Vision*, 60, 91–110.

Lucks, L., Hirt, P.-R., Hoegner, L., Stilla, U., 2022. Photogrammetric monitoring of gravitational mass movements in alpine regions by markerless 3d motion capture. *The International Archives of the Photogrammetry, Remote Sensing and Spatial Information Sciences*, XLIII-B2-2022, 1063–1069. https://isprs-archives.copernicus.org/articles/XLIII-B2-2022/1063/2022/.

Lucks, L., Stilla, U., Hoegner, L., Holst, C., 2024. Photogrammetric rockfall monitoring in Alpine environments using M3C2 and tracked motion vectors. *ISPRS Open Journal of Photogrammetry and Remote Sensing*, 12, 100058.

Morelli, L., Ioli, F., Maiwald, F., Mazzacca, G., Menna, F., Remondino, F., 2024. Deep-image-matching: a toolbox for multiview image matching of complex scenarios. *The International Archives of the Photogrammetry, Remote Sensing and Spatial Information Sciences*, XLVIII-2/W4-2024, 309–316. https://isprs-archives.copernicus.org/articles/XLVIII-2-W4-2024/309/2024/.

Ogundare, J. O., 2016. *Precision surveying: The principles and geomatics practice*. John Wiley and Sons Inc, Hoboken.

Pelzer, H., 1971. Zur Analyse geodätischer Deformationsmessungen. *Deutsche Geodätische Kommission bei der Bayerischen Akademie der Wissenschaften Reihe C: Dissertationen*.

Raffl, L., Holst, C., 2022. Including virtual target points from laser scanning into the point-wise rigorous deformation analysis at geo-monitoring applications. *Proceedings of the 5th Joint International Symposium on Deformation Monitoring (JISDM)*.

Raffl, L., Holst, C., 2024. Extending geodetic networks for geomonitoring by supervised point cloud matching. *Journal of Applied Geodesy*. https://doi.org/10.1515/jag-2024-0011.

Raffl, L., Koller, M., Holst, C., in preparation. Geodetic geomonitoring networks from terrestrial laser scans using automated patch selection.

Raffl, L., Wunderlich, T., 2020. Challenges and hybrid approaches in alpine rockslide prevention - an alarming case study. *Proceedings of the 8th INGEO International Conference on Engeneering Serveying & 4th SIG Symposium on Engeneering Geodesy*.

Strecha, C., 2014. Pix4D - Error Estimation. 1rd edn, Pix4D, Prilly, Swiss.

Winiwarter, L., Anders, K., Höfle, B., 2021. M3C2-EP: Pushing the limits of 3D topographic point cloud change detection by error propagation. *ISPRS Journal of Photogrammetry and Remote Sensing*, 178, 240–258.

Wujanz, D., Burger, M., Mettenleiter, M., Neitzel, F., 2017. An Intensity-based stochastic model for terrestrial laser scanners. *ISPRS Journal of Photogrammetry and Remote Sensing*, 125, 146–155.

Yang, Y., Schwieger, V., 2023. Patch-based M3C2: Towards lower-uncertainty and higher-resolution deformation analysis of 3D point clouds. *International Journal of Applied Earth Observation and Geoinformation*, 125, 103535.

Zahs, V., Winiwarter, L., Anders, K., Williams, J. G., Rutzinger, M., Höfle, B., 2022. Correspondence-driven plane-based M3C2 for lower uncertainty in 3D topographic change quantification. *ISPRS Journal of Photogrammetry and Remote Sensing*, 183, 541-559.